Proceedings of the Twenty-sixth (2016) International Ocean and Polar Engineering Conference **www.isope.org**
Rhodes, Greece, June 26-July 1, 2016

ISBN 978-1-880653-88-3; ISSN 1098-6189

A Reduced-Order, Statistical Linearization Approach For Estimating Nonlinear Floating Wind Turbine Response Statistics

Jocelyn M. Kluger, Themistoklis P. Sapsis, Alexander H. Slocum
Department of Mechanical Engineering, Massachusetts Institute of Technology.
Cambridge, Massachusetts, USA

ABSTRACT

An order-reduction method has been developed for efficiently estimating the steady state response of an offshore wind turbine. The method uses eigenanalysis for the tower's two lowest bending modes, statistical linearization for the nonlinear ocean wave viscous forcing and wind-induced damping, and environmental statistics for the lifetime fatigue stress. The estimated responses agree well with time-domain simulations while computing the results 100 times more efficiently. To demonstrate the method's usefulness, we use it to estimate the auxiliary power output and effects on fatigue stress of differently sized damping elements in a floating wind turbine spar platform, which represent ideal wave energy converters.

KEY WORDS: Floating wind turbine; Statistical linearization; eigenanalysis; fatigue.

INTRODUCTION

Many concepts have been considered for improving offshore wind turbine performance: different platform designs, tower and rotor types, controls, and hybrid systems with wave energy converters (Matha, 2009; Muliawan et al., 2013; Roddier et al., 2010; Slocum, 2014). Dynamics studies aid in assessing the different concepts. Wind turbines are complex systems, comprising of coupled aerodynamic, hydrodynamic, elastic, and control subsystems, which themselves contain stochasticities and nonlinearities. There are two traditional approaches to modeling wind turbine dynamics.

The first, simpler approach is a linear frequency-domain analysis (Newman, 1977; Ramachandran et al., 2013; Jonkman,2010). This dynamic model considers linear wave forcing due to potential flow, often computed by a panel method program such as WAMIT (Newman and Sclavounos, 1988). It ignores nonlinear effects related to wave viscous wave forcing or wind thrust. This method captures many important characteristics of most systems and is adequate for most preliminary design analysis (Wayman et al., 2006). The main advantage of linear frequency domain analysis is its very fast runtime for computing system steady-state responses. The limitation is that some dynamic characteristics are not captured by the model.

The second approach is a nonlinear time-domain simulation of the full system. This approach considers wave viscous forcing, usually by employing Morison elements, in addition to linear wave forcing from panel methods. For the tower and blade bending, FAST employs modal analysis while HAWC2 uses a finite element formulation where the structure is divided into Timoshenko beams connected to each other by constraints (Jonkman and Buhl, 2005; Karimirad, 2013; Larsen and Hansen, 2005). In the time domain, turbine speed and blade pitch controllers are easily simulated. The main advantages of time domain simulations are the ability to compute transient effects and responses to extreme loads that occur during storms when nonlinear viscous effects are significant (Jonkman, 2010). Even as advances are being made to accelerate the time-domain simulations by substructuring and parallel processing, the intrinsic challenge of time-domain simulations is high computation cost (Schafhirt et al., 2015).

The two methods are appropriate for different stages of design. The linear approach will always be the fastest for basic design analysis, while only time domain simulations are rigorous enough to verify if a wind turbine meets design standards (Quarton, 2005). This paper is about a middle approach in between the completely linear frequency-domain model and nonlinear time-domain model. Our goal is to efficiently perform design analyses that account for system nonlinearities. First, we describe a floating wind turbine model that can be solved in the frequency domain. The approach uses a Galerkin projection to model tower bending, statistical linearization to model nonlinear viscous wave forcing and steady wind damping, and environmental statistics to calculate tower fatigue stress. We find good agreement between our results and FAST. Then, we apply the approach to optimizing an ideal wave energy converter in the spar of a floating wind turbine. Throughout this paper, we use the National Renewable Energy Laboratory (NREL) 5-MW wind turbine mounted on the OC3 spar as a case study (Jonkman et al., 2009; Jonkman, 2010).

FREQUENCY-DOMAIN MODEL

We model the dynamics of the floating wind turbine by the linear equation of motion,

$$\mathbf{I}(\omega)\ddot{\vec{x}} + \mathbf{B}(\omega)\dot{\vec{x}} + \mathbf{K}\vec{x} = \vec{f}(\omega). \tag{1}$$

For simplicity in this paper, we consider only the coupled degrees of freedom excited by head-on incident wind and waves,

$$\vec{x} = \begin{bmatrix} x_1 \\ x_3 \\ x_5 \\ \alpha_1 \\ \alpha_2 \end{bmatrix}, \tag{2}$$

where x_1, x_3, and x_5 are the rigid platform surge, heave, and pitch motions about the mean water level, respectively, as labeled in Fig. 1. α_1 and α_2 are time-dependent coefficients of the flexible tower's first and second fore-aft bending modes. Future studies may easily expand the model to include additional degrees of freedom for the platform motion, tower side-side bending modes, and attached wave energy converter arrays. $\mathbf{I}(\omega)$, $\mathbf{B}(\omega)$, and $\mathbf{K}$ are inertia, damping, and spring stiffness matrices respectively. Throughout this paper, we refer to a coordinate system with an origin at the still water level, so the matrices contain nondiagonal terms as per the parallel axis theorem. Matrices not explicitly listed in this paper are given in Jonkman (2010). We define the inertia matrix as

$$\mathbf{I}(\omega) = \mathbf{M}_{\text{Platform}} + \mathbf{M}_{\text{Tower}} + \mathbf{A}_{\text{Hydro}}(\omega), \tag{3}$$

where $\mathbf{M}_{\text{Platform}}$ and $\mathbf{M}_{\text{Tower}}$ are the mass matrices of the rigid platform and flexible tower, respectively. $\mathbf{M}_{\text{Tower}}$ contains elements coupling the tower's bending modes and rigid heave motion with the platform. $\mathbf{A}_{\text{Hydro}}(\omega)$ is the floating platform's added mass. The damping matrix is

$$\mathbf{B}(\omega) = \mathbf{B}_{\text{Hydro}}(\omega) + \mathbf{B}_{\text{Tower}} + \mathbf{B}_{\text{Visc,eq}} + \mathbf{B}_{\text{Wind,eq}} + \mathbf{B}_{\text{WEC}}, \tag{4}$$

where $\mathbf{B}_{\text{Hydro}}(\omega)$ is the frequency-dependent platform hydrodynamic damping, $\mathbf{B}_{\text{Tower}}$ is damping related to the tower bending. $\mathbf{B}_{\text{Visc,eq}}$ and $\mathbf{B}_{\text{Wind,eq}}$ are the effective damping coefficients found by statistical linearization of the nonlinear viscous drag of water motion on the platform and wind on the rotor. $\mathbf{B}_{\text{WEC}}$ is damping due to an attached wave energy converter. The spring stiffness matrix is

$$\mathbf{K} = \mathbf{C}_{\text{Hydro}} + \mathbf{K}_{\text{Mooring}} + \mathbf{K}_{\text{Tower}}, \tag{5}$$

where $\mathbf{C}_{\text{Hydro}}$ contains the platform hydrostatic restoring coefficients, $\mathbf{K}_{\text{Mooring}}$ is the linear spring stiffness matrix representing the mooring lines, and $\mathbf{K}_{\text{Tower}}$ contains the tower stiffness coefficients. The complex-valued wave forcing vector is

$$\vec{f} = \vec{f}_{\text{Hydro}} + \vec{f}_{\text{Visc,Eq}} = \Re\text{e}\left\{\vec{F}e^{i\omega t}\right\} = \Re\text{e}\left\{\begin{bmatrix} F_1 \\ F_3 \\ F_5 \\ 0 \\ 0 \end{bmatrix} e^{i\omega t} + \begin{bmatrix} F_{1,\text{Visc,eq}} \\ 0 \\ F_{5,\text{Visc,eq}} \\ 0 \\ 0 \end{bmatrix} e^{i\omega t}\right\}, \tag{6}$$

where $\vec{f}_{\text{Hydro}}$ is the linear hydrodynamic forcing and $\vec{f}_{\text{Visc,Eq}}$ is the statistically linearized viscous forcing of the waves on the platform. The frequency-dependent values of $\mathbf{A}_{\text{Hydro}}(\omega)$, $\mathbf{B}_{\text{Hydro}}(\omega)$, and $\vec{f}_{\text{Hydro}}(\omega)$ may be obtained from a panel radiation/diffraction program such as WAMIT (Lee and Newman, 2013). The response amplitude operator of the system for waves with amplitude a and frequency ω is

$$\vec{H}(\omega) = \frac{\vec{X}}{a} = (-\omega^2\mathbf{I} + j\omega\mathbf{B} + \mathbf{K})^{-1}\frac{\vec{F}}{a}. \tag{7}$$

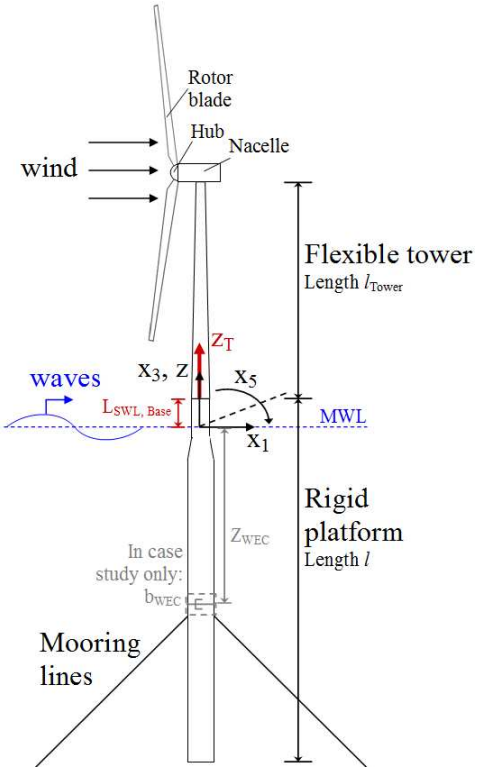

Fig. 1 Catenary moored spar floating wind turbine with head-on wind and incident waves. In our case study, we add a damping element representing an ideal wave energy converter to the platform.

Table 1 Floating wind turbine properties

Parameter	Value
Tower length, L_{Tower}	77.6 m
Distance from the SWL to the tower base, $L_{\text{SWL,Base}}$	10 m
Distance from the SWL to the tower top, $L_{\text{SWL,Top}}$	87.6 m
Tower base diameter	6.5 m
Tower base thickness	2.7 cm
Tower top diameter	3.87 m
Tower top thickness	1.9 cm
Tower top point mass, m_{Top}	3.50×10^5 Kg
Tower elastic modulus, E	210 GPa
Tower density, ρ_{Steel}	8500 Kg/m^3
Tower ultimate strength, S_{Ult}	2260 MPa
Tower Wohler parameter, m	5
Rotor moment of inertia about SWL	4.32×10^8 Kgm^2
Rotor diameter	126 m
Rotor swept area, S	1.25×10^4 m
Case study only: WEC submergence, z_{WEC}	70 m

Using the Wiener-Khinchine theorem, the power spectral density of the steady-state system is

$$S^+_{\vec{x}}(\omega) = |\vec{H}(\omega)|^2 S^+_u(\omega), \tag{8}$$

and the standard deviation in the response is

$$\sigma_{\vec{x}}(\omega) = \sqrt{\int_0^\infty S^+_{\vec{x}}(\omega)\text{d}\omega}, \tag{9}$$

where $S_u^+(\omega)$ is the ocean wave elevation single-sided spectral density (Roberts and Spanos, 1999).

Reduced order modeling of the tower bending dynamics

The differential equation for the transverse tower deflection relative to the floating platform, $u(z_T, t)$, is

$$EI(z_T)\frac{\partial^4 u}{\partial z_T^4} + \rho A(z_T)\left(\frac{\partial^2 u}{\partial t^2} + \frac{\partial^2 y(z_T,t)}{\partial t^2}\right) = 0. \tag{10}$$

For the NREL offshore 5-MW baseline wind turbine, the tower's second moment of area, $I(z_T)$, and cross sectional area, $A(z_T)$, depend on the tower coordinate, z_T, as described in Jonkman et al. (2009, 2010). Lateral tower acceleration caused by the platform acceleration, $\partial^2 y(z_T,t)/\partial t^2$, depends on the tower coordinate z_T, because of the contribution of platform pitch,

$$\frac{\partial^2 y(z_T,t)}{\partial t^2} = \frac{\mathrm{d}^2 x_1}{\mathrm{d}t^2} + (L_{SWL,Base} + z_T)\frac{\mathrm{d}^2 x_5}{\mathrm{d}t^2}, \tag{11}$$

where $L_{\mathrm{SWL,Base}} = 10$ m is the distance from the still water level to the tower base for the OC3-Hywind system.

We use the Galerkin method to convert the continuous differential equation describing the tower fore-aft bending dynamics, Eq. 10, to several discrete differential equations based on the tower's natural frequencies and corresponding eigenshapes. That is, we approximate a solution to the tower bending with the form,

$$u(t, z_T) \approx \alpha_1(t)u_1(z_T) + \alpha_2(t)u_2(z_T) + ... \tag{12}$$

Here, we consider the tower bending shapes, $u_1(z_T)$ and $u_2(z_T)$, corresponding to its two lowest natural frequencies. The higher bending modes, with frequencies exceeding 10 Hz, have negligible impact on the structure dynamics when the structure is excited by sea waves, which have frequencies less than 5 Hz.

We use ANSYS© finite element software modal analysis to numerically determine the tower's natural frequencies and corresponding bending shapes. In ANSYS, we model the tower as a cantilevered, hollow tapered cylinder with the parameters listed in Table 1. These parameters match the OC3-Hywind system (Jonkman, 2010). In ANSYS, we model the hub, nacelle, and rotor masses as a single point mass on the tower top.

ANSYS modal analysis calculates the relative lateral deformations of finite element nodes along the tower. Fig. 2 shows these eigenshapes. We use Matlab© Curve Fitting Toolbox to best-fit the nodal deformations to the curve,

$$u_i(z_T) = a_2 z_T^2 + a_3 z_T^3 + a_4 z_T^4 + a_5 z_T^5 + a_6 z_T^6. \tag{13}$$

Eq. 13 represents the eigenshape's neutral axis deformation. This eigenshape satisfies the tower's kinematic boundary conditions at the base of zero deformation ($u(0) = 0$) and slope ($\partial u(0)/\partial z_T) = 0$). Table 2 lists the coefficients for the tower's two lowest frequency bending modes. We made slight adjustments to the coefficients so that the tower's natural frequencies match those in Matha (2009). The coefficients listed in Table 2 are meaningful only for relative displacements along the tower, as we will scale and dimensionalize them with the time-dependent coefficients $\alpha_1(t)$ and $\alpha_2(t)$, respectively in Eq. 12. Future studies may use a more accurate method for determining the eigenshapes. However, we found that the above method produced accurate enough results for our analysis.

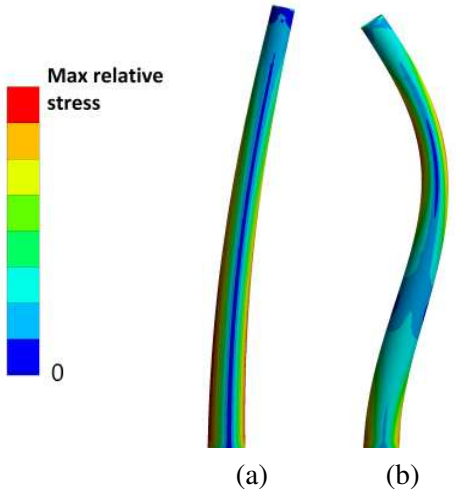

Fig. 2 Eigenshapes and von-Mises stress trends for the tower's two lowest fore-aft bending modes. (a) Mode 1, $u_1(z)$, 0.47 Hz. (b) Mode 2, $u_2(z)$, 3.75 Hz. For illustration purposes in this figure, the maximum curvature and von-Mises stress is approximately 10 times larger in Mode 2 than in Mode 1.

Table 2 Coefficients for neutral axis line-of-best-fit for the tower bending modes, $u_1(z)$ and $u_2(z)$.

Coefficient	Mode 1, $u_1(z)$, 0.47 Hz	Mode 2, $u_2(z)$, 3.75 Hz
a_2	2.95×10^{-7}	3.85×10^{-6}
a_3	-7.48×10^{-10}	-6.43×10^{-8}
a_4	2.71×10^{-11}	7.23×10^{-10}
a_5	-4.63×10^{-13}	-1.36×10^{-11}
a_6	9.89×10^{-16}	8.79×10^{-14}

Having determined the tower bending shapes, $u_1(z_T)$ and $u_2(z_T)$, we substitute the assumed solution, Eq.s 12 and 13, into the governing equation, Eq. 10,

$$EI\left(\alpha_1 u_1^{\mathrm{iv}} + \alpha_2 u_2^{\mathrm{iv}}\right) + \rho A\left(\ddot{\alpha}_1 u_1 + \ddot{\alpha}_2 u_2 + \ddot{y}\right) = 0, \tag{14}$$

where the roman numerals indicate derivatives with respect to space and dots with respect to time. To find the governing equation of the first bending mode, we multiply Eq. 14 by u_1 and integrate along z_T,

$$\int_0^l EI\left(\alpha_1 u_1^{\mathrm{iv}} u_1 + \alpha_2 u_2^{\mathrm{iv}} u_1\right)\mathrm{d}z_T + \int_0^l \rho A\left(\ddot{\alpha}_1 u_1 u_1 + \ddot{\alpha}_2 u_2 u_1 + \ddot{y} u_1\right)\mathrm{d}z_T = 0. \tag{15}$$

Using the self-adjoint and orthogonality properties of the eigenshapes, and substituting in Eq. 11 for $\ddot{y}$, Eq. 15 reduces to

$$\alpha_1\left(\int_0^l EI(u_1^{\mathrm{ii}})^2\,\mathrm{d}z_T\right) + \ddot{\alpha}_1\left(\int_0^l \rho A u_1^2 \mathrm{d}z_T\right) + \ddot{x}_1\left(\int_0^l \rho A(u_1 \mathrm{d}z_T\right) + \ddot{x}_5\left(\int_0^l \rho A(l_{SWL,Base} + z_T)u_1 \mathrm{d}z_T\right) = 0. \tag{16}$$

We define new coefficients to express Eq. 16 as,

$$k_1\alpha_1 + m_1\ddot{\alpha}_1 + m_{1,p1}\ddot{x}_1 + m_{1,p5}\ddot{x}_5 = 0. \tag{17}$$

Repeating the procedure from Eq. 14 for u_2 produces the second tower bending mode governing equation,

$$k_2\alpha_2 + m_2\ddot{\alpha}_2 + m_{2,p1}\ddot{x}_2 + m_{2,p5}\ddot{x}_5 = 0. \tag{18}$$

Table 3 lists the calculated coefficients. It is important to note that m_i, $m_{i,p1}$, and $m_{1,p5}$ account for the tower end mass.

Table 3 Bending mode coefficients and natural frequencies derived by Galerkin projection.

Coefficient	Mode 1, $f_1 = 0.47$ Hz	Mode 2, $f_2 = 3.75$ Hz
m_i	2.778×10^0	8.476×10^{-1}
k_i	2.461×10^1	4.715×10^2
$m_{i,p1}$	1.131×10^3	4.190×10^2
$m_{i,p5}$	9.432×10^4	2.364×10^4

Next, we determine the tower's influence on the platform dynamics by using the Euler-Lagrange approach. For the tower-platform system with four coupled degrees of freedom; platform surge x_1, platform pitch x_5, and two tower bending modes contained in u, given in Eq. 12; the potential energy is due to the tower bending,

$$V = \frac{E}{2}\int_0^l I(u^{ii})^2 \mathrm{d}z. \tag{19}$$

The kinetic energy is

$$T = \frac{1}{2}m_{p1}\dot{x}_1^2 + \frac{1}{2}m_{p5}\dot{x}_5^2 + m_{p15}\dot{x}_1\dot{x}_5 + \frac{1}{2}\int_0^l \rho A(\dot{x}_1 + (L_{\mathrm{SWL,Base}} + z)\,\dot{x}_5 + \dot{u})^2 \mathrm{d}z + \frac{1}{2}m_{\mathrm{Top}}(\dot{x}_1 + (L_{\mathrm{SWL,Base}} + L_{\mathrm{Tower}} + \dot{u})^2 + \frac{1}{2}I_{\mathrm{Top}}\dot{x}_5^2, \tag{20}$$

where m_{p1}, m_{p5}, and m_{p15} are the platform surge mass, pitch inertia, and product of inertia, respectively, m_{Top} is the combined hub, rotor, nacelle mass at the tower top, and I_{Top} is the rotor inertia about the SWL. Defining the Lagrangian as

$$\mathcal{L} = T - V, \tag{21}$$

and substituting Eq.s 19-21 into the equation,

$$\frac{\mathrm{d}}{\mathrm{d}t}\left(\frac{\partial \mathcal{L}}{\partial \dot{q}}\right) - \frac{\partial \mathcal{L}}{\partial q} = 0, \tag{22}$$

for $q = x_1$ and $q = x_5$ reveals coupling terms between the platform and tower. The final tower mass and stiffness matrices are

$$\mathbf{M}_{Tower} = \begin{bmatrix} 6.02\times10^5 & 0 & 4.16\times10^7 & 1.13\times10^3 & 4.19\times10^2 \\ 0 & 6.02\times10^5 & 0 & 0 & 0 \\ 4.16\times10^7 & 0 & 3.32\times10^9 & 9.43\times10^4 & 2.36\times10^4 \\ 1.13\times10^3 & 0 & 9.43\times10^4 & 2.78\times10^0 & 0 \\ 4.19\times10^2 & 0 & 2.36\times10^4 & 0 & 8.48\times10^{-1} \end{bmatrix} \mathrm{Kg}, \tag{23}$$

$$\mathbf{K}_{Tower} = \begin{bmatrix} 0 & 0 & 0 & 0 & 0 \\ 0 & 0 & 0 & 0 & 0 \\ 0 & 0 & 0 & 0 & 0 \\ 0 & 0 & 0 & 2.46\times10^1 & 0 \\ 0 & 0 & 0 & 0 & 4.71\times10^2 \end{bmatrix} \mathrm{N/m}. \tag{24}$$

Statistical linearization of wave viscous forcing

Viscous forces play a significant role in rough sea states (Jonkman, 2010). Using Morison's equation to approximate viscous forcing on the spar platform, the surge force and pitch moment are

$$\vec{F}_D = \begin{bmatrix} F_{D1} \\ 0 \\ F_{D5} \\ 0 \\ 0 \end{bmatrix} = \begin{bmatrix} \frac{1}{2}\rho C_D \int_T^0 D\,\dot{q}\,|\dot{q}|\,\mathrm{d}z \\ 0 \\ -\frac{1}{2}\rho C_D \int_T^0 zD\,\dot{q}\,|\dot{q}|\,\mathrm{d}z \\ 0 \\ 0 \end{bmatrix}, \tag{25}$$

where we use the viscous drag coefficient, $C_D = 0.6$ (Jonkman, 2010). We define the total horizontal velocity of the water relative to the platform as

$$\dot{q} = V_{\mathrm{water}} - V_{\mathrm{platform}} = \sum_j^n \Re\mathrm{e}\left(\left\{\frac{-a_j k_j g}{\omega_j}\frac{\cosh k_j(z+h)}{\cosh k_j h} - \omega_j X_{1j} - z\omega_j X_{5j}\right) e^{i(\omega_j t + \phi_j)}\right\}, \tag{26}$$

where h is the water depth and $\dot{q}$ is a function of the depth below the water, z. Future work will increase the accuracy of V_{water} by accounting for radiation and diffraction effects. We sum n ocean wave and platform response harmonics. For each harmonic, ϕ_j is a random variable with a uniform distribution for $0 \le \phi_j \le 2\pi$. The Central Limit Theorem guarantees that $\dot{q}$ will be a Gaussian stochastic process for large n. As described in Roberts and Spanos (1999), we may determine statistically equivalent linear damping coefficients in the surge and pitch modes of the form

$$\mathbf{B}_{\mathrm{Visc,eq}} = \begin{bmatrix} -E\left\{\frac{\partial F_{D1}}{\partial \dot{x}_1}\right\} & 0 & -E\left\{\frac{\partial F_{D1}}{\partial \dot{x}_5}\right\} & 0 & 0 \\ 0 & 0 & 0 & 0 & 0 \\ -E\left\{\frac{\partial F_{D5}}{\partial \dot{x}_1}\right\} & 0 & -E\left\{\frac{\partial F_{D5}}{\partial \dot{x}_5}\right\} & 0 & 0 \\ 0 & 0 & 0 & 0 & 0 \\ 0 & 0 & 0 & 0 & 0 \end{bmatrix}, \tag{27}$$

where $E\{\}$ is the expectation of the Gaussian process. Substituting Eq.s 25 and 26 into Eq. 27, we obtain,

$$\mathbf{B}_{\mathrm{Visc,eq}} = \begin{bmatrix} \rho C_D \int_T^0 D(z)\,E\{|\dot{q}(z)|\}\,\mathrm{d}z & 0 & \rho C_D \int_T^0 zD(z)\,E\{|\dot{q}|\}\,\mathrm{d}z & 0 & 0 \\ 0 & 0 & 0 & 0 & 0 \\ -\rho C_D \int_T^0 zD(z)\,E\{|\dot{q}|\}\,\mathrm{d}z & 0 & -\rho C_D \int_T^0 z^2 D(z)\,E\{|\dot{q}|\}\,\mathrm{d}z & 0 & 0 \\ 0 & 0 & 0 & 0 & 0 \\ 0 & 0 & 0 & 0 & 0 \end{bmatrix}. \tag{28}$$

The Gaussian process $\dot{q}$ has a probability density of the form,

$$f_{\dot{Q}}(\dot{q}) = \frac{1}{\sqrt{2\pi}\sigma_{\dot{q}}} e^{-\frac{(\dot{q}-\bar{\dot{q}})^2}{2\sigma_{\dot{q}}^2}}, \tag{29}$$

where $\sigma_{\dot{q}}$ is the random variable's standard deviation and its mean $\bar{\dot{q}} = 0$. Then, the expected value of $|\dot{q}|$ is

$$E\{|\dot{q}|\} = \int_{-\infty}^{\infty} |\dot{q}| f_{\dot{Q}}(\dot{q})\,\mathrm{d}\dot{q} = \frac{\sqrt{2}\sigma_{\dot{q}}}{\sqrt{\pi}}. \tag{30}$$

The statistically equivalent viscous wave forcing is

$$\vec{F}_{\text{Visc,eq}} = \int_T^0 \left(E\left\{ \frac{\partial \vec{F}_D}{\partial V_{Water}} \right\} V_{Water} \right) \mathrm{d}z$$
$$= \begin{bmatrix} \rho C_D \int_T^0 \left(D(z) E\left\{ |\dot{q}(z)| \right\} V_{Water} \right) \mathrm{d}z \\ 0 \\ -\rho C_D \int_T^0 \left(z D(z) E\left\{ |\dot{q}(z)| \right\} V_{Water} \right) \mathrm{d}z \\ 0 \\ 0 \end{bmatrix}, \quad (31)$$

(Roberts and Spanos, 1999). In our frequency-domain method of calculating the floating wind turbine response, we iteratively solve for $\mathbf{B}_{\text{Visc,eq}}$ and $\vec{F}_{\text{Visc,eq}}$ until the system response, $\sigma_{\vec{X}}$ converges to within 0.1%, which typically requires less than 4 iterations for the OC3 spar.

Statistical linearization of nonlinear steady wind forcing

Similarly to the wave viscous forcing, we statistically linearize the forcing on the platform due to a steady wind flowing past the rotor. The steady wind forcing is nonlinear because platform motion moves the hub, which changes the incident wind speed relative to the hub. The nonlinear forcing on the platform is

$$\vec{F}_T = \begin{bmatrix} F_{T1} \\ 0 \\ F_{T5} \\ 0 \\ 0 \end{bmatrix} = \begin{bmatrix} \frac{1}{2}\rho_a C_T S\, \dot{q}_W\, |\dot{q}_W| \\ 0 \\ \frac{1}{2}\rho_a C_T S\, L_{\text{SWL,Top}}\, \dot{q}_W\, |\dot{q}_W| \\ 0 \\ 0 \end{bmatrix}, \quad (32)$$

where $L_{\text{SWL,Top}}$ is the distance from the still water level to the tower top, $S = \pi D_{Rotor}^2/4$ is the swept rotor area. We base our rotor thrust coefficient, $C_T(V_{Wind})$, on the steady-state thrust force given in Jonkman et al. (2009),

$$C_T = \frac{F_{\text{Thrust}}(V_{\text{Hub}})}{\frac{1}{2}\rho_a S V_{\text{Hub}}^2}, \quad (33)$$

as plotted in Fig. 3. We use air density ρ_a= 1.225 Kg/m^3. We define the horizontal velocity of the wind relative to the tower top as

$$\dot{q}_W = V_{wind} - V_{top} = \overline{V}_{Wind} - \dot{x}_1 - L_{\text{SWL,Top}} \dot{x}_5. \quad (34)$$

$\overline{V}_{Wind}$ is the constant wind speed in a given wind-sea state. The statistically equivalent linear damping coefficients due to the wind flow have the form (Roberts and Spanos, 1999)

$$\mathbf{B}_{\mathbf{Wind,eq}} = \begin{bmatrix} -E\left\{\frac{\partial F_T}{\partial \dot{x}_1}\right\} & 0 & -E\left\{\frac{\partial F_T}{\partial \dot{x}_5}\right\} & 0 & 0 \\ 0 & 0 & 0 & 0 & 0 \\ -E\left\{\frac{\partial M_T}{\partial \dot{x}_1}\right\} & 0 & -E\left\{\frac{\partial M_T}{\partial \dot{x}_5}\right\} & 0 & 0 \\ 0 & 0 & 0 & 0 & 0 \\ 0 & 0 & 0 & 0 & 0 \end{bmatrix}. \quad (35)$$

Substituting Eq.s 32 and 34 into Eq. 35, we obtain,

$$\mathbf{B}_{\mathbf{Wind,eq}} = \begin{bmatrix} \rho_a C_T S\, E\{|\dot{q}_W(z)|\} & 0 & \rho_a C_T L_{\text{SWL,Top}} S\, E\{|\dot{q}_W|\} & 0 & 0 \\ 0 & 0 & 0 & 0 & 0 \\ \rho_a C_T L_{\text{SWL,Top}} S\, E\{|\dot{q}_W|\} & 0 & \rho_a C_T L_{\text{SWL,Top}}^2 S\, E\{|\dot{q}_W|\} & 0 & 0 \\ 0 & 0 & 0 & 0 & 0 \\ 0 & 0 & 0 & 0 & 0 \end{bmatrix}, \quad (36)$$

where for steady wind speed $\overline{V}_{Wind}$, the expected value of $|\dot{q}_W|$ is

$$E\{|\dot{q}_W|\} = \int_{-\infty}^{\infty} |\dot{q}_W| f_{\dot{Q}_W}(\dot{q}_W)\, \mathrm{d}\dot{q}_W = \frac{\sqrt{2}\sigma_{\dot{q}_W}}{\sqrt{\pi}} e^{-\overline{V}^2/2\sigma_{\dot{q}_W}^2} + \overline{V}_{Wind} \mathrm{erf}\left(\frac{\overline{V}_{Wind}}{\sqrt{2}\sigma_{\dot{q}_W}} \right).$$

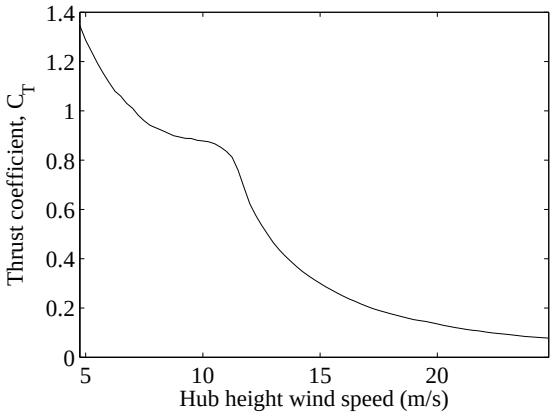

Fig. 3 Assumed turbine thrust coefficient, $C_T = \frac{F_{\text{Thrust}}}{0.5\rho_a S V^2}$, versus wind speed, V, derived from Jonkman et al. (2009).

(37)

When the wind's fluctuating component can be neglected, its statistically linearized forcing on the oscillating wind turbine is a constant value (Roberts and Spanos, 1999),

$$\vec{F}_{\text{Wind,eq}} = E\left\{\vec{F}_T\right\} = \begin{bmatrix} 1 \\ 0 \\ L_{\text{SWL,Top}} \\ 0 \\ 0 \end{bmatrix} \frac{1}{2}\rho_a C_T S \overline{V}^2. \quad (38)$$

Fatigue stress based on statistics

Traditional time-domain simulations rainflow-count the alternating stress cycles over a structure lifetime to determine the equivalent fatigue stress (EFS) (Robertson and Jonkman, 2009; Matha, 2009). For known environmental data of an offshore site wave-wind states, we combine statistics with our frequency-domain dynamic model to calculate the EFS at the tower base due to wave excitation and steady wind (Naess and Moan, 2013).

As the tower vibrates in its two lowest frequency bending modes, the maximum tensile stress at the tower base is

$$s_{\text{Base,Max}} = 0.43\alpha_1(t) + 4.2\alpha_2(t)\,\text{MPa}, \quad (39)$$

where we use the results from ANSYS modal analysis. Using results from ANSYS static analysis, the thrust force on the rotor due to steady wind causes an additional mean stress on the tower base,

$$s_{\text{Base,Thrust}} = \overline{s} = 9.03 \times 10^{-2} F_{Thrust}\,(V_{Hub})\ \text{MPa}, \quad (40)$$

where the rotor thrust force, F_{Thrust}, in units of kN, is a function of the hub-height wind speed as given in Jonkman et al. (2009).

For a given sea and wind state, the tower bending is considered a stationary, narrow-banded Gaussian process, allowing us to approximate the fluctuating stress peaks, s_P, from Eq. 39, with a Rayleigh probability density,

$$f_{S_p}(s_p) = \frac{s_p}{\sigma_{Sp}^2} e^{\frac{-s_p^2}{2\sigma_{Sp}^2}},\ s_p > 0, \quad (41)$$

where σ_{S_p} is the standard deviation of the stress. We approximate the stress cycle period as,

$$T_z = 2\pi \frac{\sigma_{S_p}}{\dot{\sigma}_{S_p}}, \tag{42}$$

where

$$\dot{\sigma}_{S_p} = \sqrt{\int_0^\infty \omega^2 S^+_{S_p}(\omega) \mathrm{d}\omega}. \tag{43}$$

The wave-induced stress power spectral density is

$$S^+_{S_p}(\omega) = |0.43 H_{\alpha_1}(\omega) + 4.2 H_{\alpha_2}(\omega)|^2 S^+_u, \tag{44}$$

where $H_{\alpha_1}(\omega)$ and $H_{\alpha_2}(\omega)$ are the transfer functions of the tower bending coefficients and S^+_u is the ocean power spectral density, from Eq.s 7-8 and 40. We approximate the number of cycles of a certain stress amplitude and mean $(s_p, \bar{s})$ during each wind/sea state as,

$$n_{\mathrm{State},s_p,\bar{s}} \approx f_{S_p}(s_p)\, \Delta S_p \frac{T_{\mathrm{State}}}{T_z}, \tag{45}$$

where ΔS_p is the stress peak step-width used in our numerical summation, and the time spent in a given sea state over the device lifetime is

$$T_{\mathrm{State}} = p_{\mathrm{State}} T_{\mathrm{Life}}. \tag{46}$$

We base p_{State}, the fraction of the device's lifetime, T_{Life}, when the structure is in a certain wind-sea state, on historical site data.

From Basquin's equation, the number of cycles to fatigue failure for a stress mean/peak pair is (Dowling, 2007)

$$N_F = \frac{1}{2}\left(\frac{s_{Ult} - |\bar{s}|}{s_p}\right)^m. \tag{47}$$

where for the steel material properties, we use ultimate stress, s_{Ult} = 2260 MPa, and Wohler parameter $m = 5$, which are limits used by Matha (2009). Using the Palmgren-Miner Rule, the damage incurred over the device lifetime is

$$D_{\mathrm{Life}} = \sum_{\mathrm{States}} \sum_{s_p,\bar{s}\ \mathrm{pairs}} \frac{n_{State,s_p,\bar{s}}}{N_F}, \tag{48}$$

where $D \geq 1$ indicates likely device failure.

The equivalent fatigue stress (EFS) is the constant peak-peak stress amplitude applied over the entire turbine lifetime that causes the same accumulated damage as caused by the stochastic loads. Rearranging Eq.s 45-48 shows

$$EFS = 2\left(\frac{D_{\mathrm{Life}}}{2n_{\mathrm{Life}}}\right)^{1/m} (\sigma_{\mathrm{Ult}} - |\bar{s}_{\mathrm{Life}}|), \tag{49}$$

where n_{Life} is the total stress cycles over the device's lifetime,

$$n_{\mathrm{Life}} = \sum_{\mathrm{States}} \frac{T_{\mathrm{State}}}{T_z}, \tag{50}$$

and $\bar{s}_{\mathrm{Life}}$ is the weighted mean stress over the device's lifetime,

$$\bar{s}_{\mathrm{Life}} = \sum_{\mathrm{States}} p_{\mathrm{State}} \bar{s}_{\mathrm{State}}. \tag{51}$$

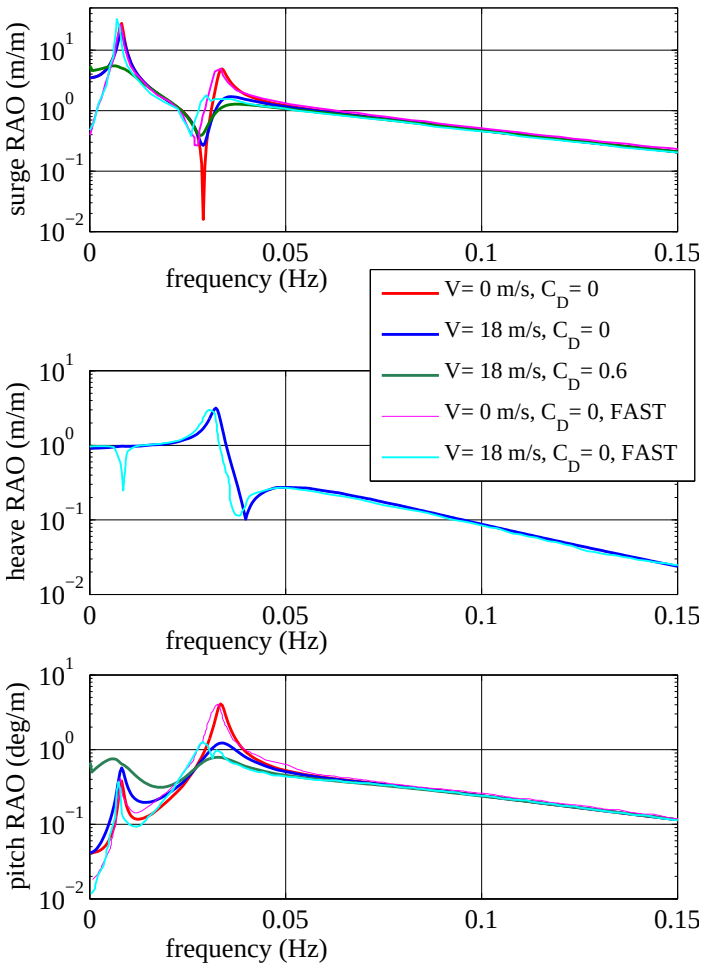

Fig. 4 Response amplitude operators for the OC3-Hywind system calculated by the nonlinear frequency domain method and FAST in (Top) surge, (Middle) heave, and (Bottom) pitch, for wind speeds $V = 0$ m/s and $V = 18$ m/s, with and without viscous effects ($C_D = 0$ or $C_D = 0.6$). The viscous effects were calculated for a Bretschneider sea state with a significant wave height, $H_s = 11$ m and dominant wave period, $T = 17$ s. The FAST results are reproduced from Ramachandran et al. (2013). All results are for a flexible tower.

RAO and EFS comparison to FAST for OC3-Hywind

First, we use the nonlinear frequency-domain approach to compute the response amplitude operators (RAO's) of the OC3-Hywind 5-MW wind turbine. We use a Galerkin projection to model the tower bending and a statistical linearization to model the nonlinear viscous wave forces and wind thrust. Our steady-state results agree well with FAST and compute the results approximately 100 times more efficiently (Ramachandran et al., 2013).

Fig. 4 shows the RAO results in surge, heave, and pitch. As labeled in Fig. 4, we consider the different modeling cases of no wind or viscous wave forces ($V = 0$, $C_D = 0$), moderate wind ($V = 18$ m/s, $C_D = 0$), and moderate wind with wave viscous forces ($V = 18$ m/s and $C_D = 0.6$). Because our model currently uncouples the heave degree of freedom from the other modes, its RAO does not change with wind speed. FAST shows only minor differences in the

heave response for different wind speeds. All of the cases shown are for a flexible tower. We compare our results with the time-domain RAO's from FAST for the cases of no wind ($V = 0$, $C_D = 0$) and steady wind ($V = 18$ m/s, $C_D = 0$) from Ramachandran et al. (2013).

There is good agreement in the responses computed by the nonlinear frequency domain approach and the FAST time-domain simulation. The differences in the $V = 18$ m/s peak frequencies (our 0.036 Hz versus Ramachandran's 0.030 Hz) are likely due to our assumed effective thrust coefficient, shown in Fig. 3, differing from Ramachandran's. Other minor differences between the responses, such as our model showing a pitch RAO>1 at 0 Hz, and the heave RAO missing a drop in value at 0.008 Hz (the surge resonance frequency) may be due to our model not considering the platform's other degrees of freedom, not coupling heave with the other modes, or having minor parameter differences.

Additionally, we plot the platform response for a loading case with viscous wave forcing (steady wind speed $V = 18$ m/s, Bretschneider sea spectrum with a significant wave height $H_s = 11$ m and dominant wave period $T = 17$ s). As expected, for the deep-draft OC3 spar platform, viscous effects generally decrease the platform response, except for a slight increase in pitch response at low frequencies ($f < 0.03$ Hz).

Finally, we compare the equivalent fatigue stress of our nonlinear frequency domain method to the EFS found by Matha (2009) using time-domain simulations with stress rainflow counting in FAST (Dowling, 2007). Matha simulated the OC3-Hywind system as experiencing 11 JONSWAP wind-sea states throughout its 20-year lifetime with wind speeds ranging from 4 to 24 m/s, significant wave heights ranging from 1.6 to 5.9 m, and dominant wave periods ranging from 9.2 to 15.5 seconds (Jonkman, 2007). For this environment, our nonlinear frequency domain method calculates an EFS of 44.5 MPa, which is within 12% of the 50.5 MPa value based on time-domain simulations (Matha, 2009). Some of the difference may be due to slight differences between our and Matha's tower and wind-sea state parameters. Although Matha accounts for wind turbulence and we model only steady wind, Karimirad (2012) shows that wind turbulence has a negligible effect on tower base bending stress. Future work will include further investigation of the EFS error.

CASE STUDY: PARAMETER OPTIMIZATION FOR AN IDEAL DAMPER IN THE OC3-HYWIND SPAR BUOY

To demonstrate an application of the nonlinear frequency domain model, we consider the simple case of an ideal wave energy converter (WEC) placed in the OC3 spar buoy, as shown in Fig 1. We model the system as experiencing 22 wind-sea states throughout its lifetime, listed in Table 4, based on historical data from a buoy 17 nautical miles WSW of Eureka, CA (NOAA, 2016). We model the WEC as a damper of spar lateral motion with a constant coefficient, b_{WEC}. This damper could be physically realized by a hydrokinetic turbine. We assume that the WEC is located at a depth $z_{\mathrm{WEC}} = -70$ m that is deep enough so that water motion due to incident waves is negligible. The model uses the WEC damping matrix,

$$\mathbf{B}_{\mathrm{WEC}} = \begin{bmatrix} b_{\mathrm{WEC}} & 0 & b_{\mathrm{WEC}} z_{\mathrm{WEC}} & 0 & 0 \\ 0 & 0 & 0 & 0 & 0 \\ b_{\mathrm{WEC}} z_{\mathrm{WEC}} & 0 & b_{\mathrm{WEC}} z_{\mathrm{WEC}}^2 & 0 & 0 \\ 0 & 0 & 0 & 0 & 0 \\ 0 & 0 & 0 & 0 & 0 \end{bmatrix}. \quad (52)$$

The WEC power is

$$P_{\mathrm{WEC}} = b_{\mathrm{WEC}} (\dot{x}_1 - z_{\mathrm{WEC}} \dot{x}_5)^2. \quad (53)$$

Table 4 Sea and wind states used in the WEC case study based on Eureka, CA NOAA buoy data from 2005-2014. H_S is the significant wave height, T_P is the dominant wave period, $\overline{V}$ is the mean wind speed, and p is the state occurence probability. We model the sea conditions by the Bretschneider spectrum.

State	H_S (m)	T_P (s)	$\overline{V}$ (m/s)	p
1	0.5	31.4	2	7.1×10^{-3}
2	0.5	15.7	2	2.1×10^{-2}
3	0.5	10.5	2	1.2×10^{-2}
4	0.5	7.85	2	1.3×10^{-2}
5	1	31.4	4	4.0×10^{-2}
6	1	15.7	4	2.2×10^{-1}
7	1	10.5	4	1.7×10^{-1}
8	1	7.85	4	9.8×10^{-2}
9	2.5	31.4	10	2.9×10^{-2}
10	2.5	15.7	10	1.9×10^{-1}
11	2.5	10.5	10	9.1×10^{-2}
12	2.5	7.85	10	2.7×10^{-2}
13	4	31.4	16	8.5×10^{-3}
14	4	15.7	16	4.7×10^{-2}
15	4	10.5	16	9.5×10^{-3}
16	4	7.85	16	1.1×10^{-3}
17	5	31.4	20	5.2×10^{-3}
18	5	15.7	20	1.2×10^{-2}
19	5	10.5	20	1.5×10^{-3}
20	5	7.85	20	5.0×10^{-5}
21	6	31.4	24	6.6×10^{-5}
22	6	15.7	24	5.0×10^{-5}

We use the nonlinear frequency domain model, with tower bending and nonlinear wind and wave forces, to calculate the average annual WEC power and lifetime equivalent fatigue stress at the tower base, as shown in Fig. 5. This method and its results allow us to quickly compare the effect of different WEC damping coefficients on device performance. We observe that a damping coefficient of 7.3×10^6 Ns/m produces the maximum power output of 7.6 kW, which is perhaps useful for an auxiliary power device, (Slocum, 2014). Damping coefficients less than 1.0×10^6 Ns/m have negligible effect on the equivalent fatigue stress while damping coefficients greater than 3.0×10^7 Ns/m approach an asymptotic limit that reduces the stress by 17%.

CONCLUSIONS

We derived a reduced-order model that computes the floating wind turbine steady-state response to nonlinear viscous wave forcing and wind damping, and lifetime equivalent fatigue stress due to tower bending in the frequency domain. The results agree well with FAST steady state results (Ramachandran, 2013). The most important advantage of this nonlinear frequency domain approach is its computational efficiency. Our nonlinear frequency domain approach computed each RAO in less than 7.5 seconds when each RAO contained 500 frequency steps and the calculation was performed using 32-bit Matlab. Obtaining the FAST RAO's required running the floating wind turbine system for 8,000 simulated seconds. For a typical FAST (simulated time):(processor time) ratio of 10, the FAST simulation required 13 minutes runtime. The nonlinear frequency approach is approximately 100 times more efficient than FAST for the RAO computation. This approach may be especially

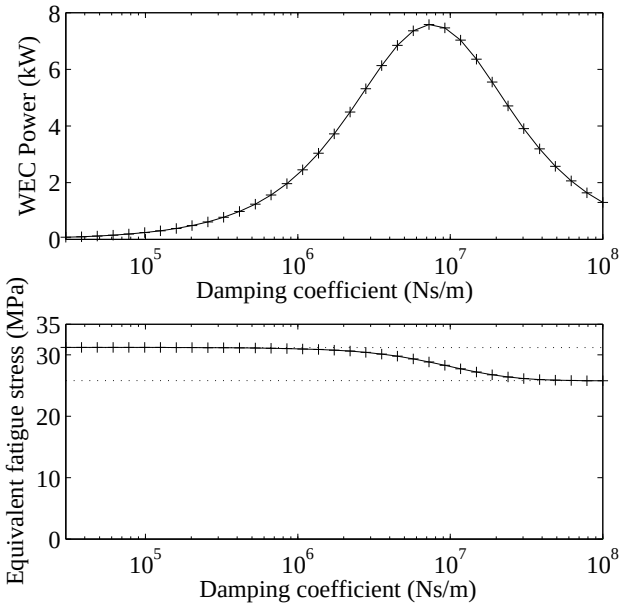

Fig. 5 WEC power and tower base lifetime effective fatigue stress for varied WEC effective damping coefficients, b_{WEC}. The WEC is submerged to $z_{WEC} = -70$ m, and the system uses the OC3-Hywind system (Jonkman, 2010).

useful for rapid design parameter optimization when nonlinear effects are important.

Future work will include expanding the model to incorporate controls, turbulent wind, additional degrees of freedom such as the rotor blades, and misaligned incident wind and wave forcing. We will apply the model to assessing the stress and auxiliary power of combined floating wind turbine-wave energy converter designs.

ACKNOWLEDGMENTS

We gratefully acknowledge the National Science Foundation for support of JMK through the Graduate Research Fellowship Program under Grant No. 1122374. We also gratefully acknowledge support by the MIT Energy Initiative through the project, 'Efficient nonlinear energy harvesting from broad-band vibrational sources by mimicking turbulent energy transfer mechanisms.'

REFERENCES

Dowling, N (2007). "Mechanical behavior of materials ", Pearson Prentice Hall, 391-455.

Jonkman, J and Buhl, M (2005). "FAST user's guide", Technical Report NREL/EL-500-38230, National Renewable Energy Laboratory, Golden, CO, 31.

Jonkman, J (2007). "Dynamics modeling and loads analysis of an offshore floating wind turbine", Technical Report NREL/TP-500-41958, National Renewable Energy Laboratory, Golden, CO, 233.

Jonkman, J, Butterfield, S, Musial, W, and Scott, G (2009). "Definition of a 5-MW reference wind turbine for offshore system development", Technical Report NREL/TP-500-47535, National Renewable Energy Laboratory, Golden, CO, 75.

Jonkman, J (2010). "Definition of the floating system for phase IV of OC3", Technical Report NREL/TP-500-47535, National Renewable Energy Laboratory, Golden, CO, 31.

Karimirad, M (2012). "Wave and wind induced dynamic response of a spar type offshore wind turbine ", *J. waterway, Port, Coastal, and Ocean Engineering*, 138, 9-20.

Karimirad, M (2013). "Modeling aspects of a floating wind turbine for coupled wave-wind-induced dynamic analyses ", *Renewable Energy*, 53, 299-305.

Larsen, T and Hansen, A (2005). "How 2 HAWC2, the user's manual", Riso National Laboratory, Denmark, 70.

Lee, C, and Newman, J (2010). "WAMIT User Manual, Version 7.062", WAMIT, Inc., 360.

Matha, D (2009). "Model development and loads analysis of an offshore wind turbine on a tension leg platform, with a comparison to other floating turbine concepts ", Technical Report NREL/SR-500-44891, National Renewable Energy Laboratory, Golden, CO, 129.

Muliawan, M, Karimirad, M, Moan, T (2013). "Dynamic response and power performance of a combined spar-type floating wind turbine and coaxial floating wave energy converter ", *Renewable Energy*, 50, 47-57.

Naess, A, and Moan, T (2013). "Stochastic Dynamics of Marine Structures", Cambridge University, 405.

Newman, J (1977). "Marine Hydrodynamics", MIT, 401.

Newman, J, Sclavounos, P (1988). "The computation of wave loads on large offshore structures ", *Proceedings of BOSS*, Trondheim, Norway, ISOPE, 18.

NOAA (2016, January 20). "Station 46022- Eel River- 17 NM WSW of Eureka, CA. "*NOAA National Data Buoy Canter*, ndbc.noaa.gov.

Ramachandran, G, Robertson, A, Jonkman, J, and Masciola, M (2013). "Investigation of response amplitude operators for floating offshore wind turbines", *Proceedings of the International Society of Offshore and Polar Engineers Conference*, Anchorage, ISOPE, 10.

Roberts, J, and Spanos, P (2003). "Random vibration and statistical linearization", Dover, 446.

Robertson, A and Jonkman, J (2009). "Loads analysis of several offshore floating wind turbine concepts", *Proceedings of the International Society of Offshore and Polar Engineers Conference*, Maui, ISOPE, 1, 8.

Roddier, D, Cermelli, C, Aubault, A, and Weinstein, A (2014). "WindFloat: A floating foundation for offshore wind turbines ", *Journal of Renewable and Sustainable Energy*, 2, 033104.

Schafhirt, S, Verkaik, N, Salman, Y, Muskulus, M (2015). "Ultra-fast analysis of offshore wind turbine support structures using impulse based substructuring and massively parallel provessors ", *Proceedings of the International Society of Offshore and Polar Engineers Conference*, Kona, Hawii, ISOPE, 1, 8.

Slocum, A (2014). "Symbiotic offshore energy harvesting and storage systems ", *Proceedings of the Offshore Energy and Storage Symposium*, Windsor, Ontario UWCAES Society, 6.

Wayman, E, Sclavounos, P, Butterfield, S, Jonkman, J, Musial, W (2006). "Coupled dynamic modeling of floating wind turbine systems ", *Proceedings of the Offshore Technology Conference*, Houston, 22.

Quarton, D (2005). "An international design standard for offshore wind turbines: IEC 61400-3 ", *Proceedings of Seacon*, Copenhagen, 10.